Available online at www.sciencedirect.com
ScienceDirect
Journal of Sound and Vibration 314 (2008) 616–634
JOURNAL OF SOUND AND VIBRATION
www.elsevier.com/locate/jsvi

Effects of variable pass speed on wear-type corrugation growth

P.A. Bellette*, P.A. Meehan, W.J.T. Daniel

CRC for Railway Engineering and Technology (Rail CRC), School of Engineering, University of Queensland, Brisbane, Qld 4072, Australia

Received 20 March 2007; received in revised form 9 November 2007; accepted 31 December 2007
Handling Editor: J. Lam
Available online 4 March 2008

Abstract

A feedback model for wear-type rail corrugation has been modified to account for vehicle speed variations over successive passages, so that the effect on corrugation amplitude growth can be investigated. The feedback model encapsulates the most critical interactions occurring between the wheel/rail structural dynamics, rolling contact mechanics and rail wear. Using this model, numerical and analytical investigations are performed to quantitatively identify the effect of deliberately changing the speed of successive vehicle passages in a statistically controlled manner. The effect of different initial track profiles on the results is also investigated. The results provide insight into a possible alternative means of retarding wear-type corrugation growth.
© 2008 Elsevier Ltd. All rights reserved.

1. Introduction

Rail corrugation is a significant problem for the railway industry worldwide. The type of corrugation on which this paper focuses is known as wear-type rail corrugation and is a particular concern to industry. Rail corrugation is a periodic irregularity that is observed to develop on the running surface of the rail with use. It is characterised by long (100–400 mm) and short (25–80 mm) wavelengths. This irregularity grows in amplitude as a function of the number of passes, until removal by grinding is required to ameliorate the excessive noise, vibration and associated problems caused by the corrugated rail. This grinding is expensive and represents a substantial cost to the railway industry [1]. There have been some techniques suggested to delay the onset of corrugations, such as rail hardfacing, but a reliable remedy, other than grinding, remains elusive.

The high cost associated with removing corrugations has motivated much research into the prediction and prevention of corrugation. Research in Germany [2], Sweden [3], Japan [4] and elsewhere has resulted in the development of simulation methods which make use of complex finite element simulations of the track dynamics along with numerical models of the rolling contact mechanics. These models are useful in that they have successfully modelled the development of corrugations and also led to the identification of behaviour that is characteristic of corrugation formation. Recently published results can give an idea of the level of sophistication attained by such advanced models. For example, Gomez et al. [5] provides a review of recent

*Corresponding author. Tel.: +61 7 3365 4179; fax: +61 7 3365 4799.
E-mail address: p.bellette@uq.edu.au (P.A. Bellette).

0022-460X/$ - see front matter © 2008 Elsevier Ltd. All rights reserved.
doi:10.1016/j.jsv.2007.12.038

efforts in the comprehensive modelling of track dynamics using numerical algorithms and provides a finite strip method for calculating the dynamics of the rail. Wu and Thompson [6] give a frequency domain model which allows for the wave interaction between subsequent wheelsets and also for the change in effective contact radius as the wheel moves along the corrugated rail profile. Jin et al. [7], provides a numerical model for corrugation formation which includes non-Hertzian rolling contact theory with a model for the lateral and vertical dynamics of a half-car traversing a curved track. This modelling seems to indicate corrugation initiation is possible from sleeper passing effects only and that the leading wheelset of the bogie is the most significant in causing corrugations. Andersson and Johansson [8] give details of a model that consists of two wheelsets and a bogie frame combined with two rails with discrete support based on finite element modelling. The contact model is based on the FASTIM algorithm [9]. A result indicated by this model that is relevant to the work in this paper is that changing the vehicle speed seems to change the wavelength of corrugation formation. One shortcoming of such models, however, is the excessive computational expense of performing parametric investigations into trends that may reduce corrugation formation. It is thought that this limitation may be overcome by simpler analytic models of corrugation formation.

Progress on analytical modelling of the growth of wear-type rail corrugation has been achieved by a number of authors over the past 50 years (see Sato et al. [1] for a comprehensive review). Modern examples of such models can be found in the work of Bhaskar et al. [10], Muller [11] and Nielson [12]. In Refs. [11,12] the effect of including nonlinear contact mechanics on the development of wear-type corrugation was discussed. Analytical predictions showed that certain wavelength ranges of corrugation were promoted due to a wavelength-based contact filtering effect. However, the effects of dynamic wheel/rail contact forces were ignored. In Refs. [10,11] investigations were performed into the stability of the interaction between structural dynamics and contact mechanics. Both of these studies predicted stable systems using realistic parameters; however, they only considered the system behaviour over one wheelset passage. In Meehan et al. [13] the interaction of the structural dynamics and contact mechanics over multiple wheelset passages was successfully investigated. This showed that there was instability and hence exponential growth of corrugations over multiple passages and a closed-form analytic expression for this growth rate was obtained. The growth rate predictions of this model were then validated against a comprehensive finite element model. The effect of variable pass speeds on corrugation growth has not been investigated, however and shall be addressed in this paper.

The model described in this paper builds upon the analytical model described in Meehan et al. [13], however, the effect of wheel pass frequency is not considered, i.e. it is assumed that the dynamics of the previous wheel pass have died away before the current wheel pass occurs. This is similar to the infinite pass delay model used in Song and Meehan [14]. It has been altered in this paper so as to account for different train speeds on consecutive passes. This should not be confused with varying speed, i.e. accelerating or decelerating during each pass, which is not considered here. This model uses a multiple degree of freedom modal description of the wheel and rail dynamics, a linear contact mechanics model and a feedback mechanism where the rail profile exiting a wheel passage is fed into the next wheelset passage. It allows for an investigation into any reduction in growth rate that may be achieved by using different pass speed distributions, for a range of initial track profiles. These results provide insight into a possible method for reducing corrugation growth.

In particular the major contributions of this paper are:

- The development of analytic solutions for the detailed rail profile history for a range of input profiles, where the vehicle speed changes on each pass.
- The development of a useful expression for quantifying the corrugation growth rate due to a distribution of train speeds. Using this expression an investigation into how different speed distribution shapes affect the corrugation growth rate has been provided.
- A theoretical proof that maximum corrugation growth rate occurs under constant pass speed conditions.
- The development of a closed-form expression of the error in growth rate induced by artificially accelerating the wear coefficient during numerical simulations.

To this end, a model of corrugation growth under the conditions of a probabilistic distribution of pass speeds will be presented. From this model, analytical solutions for the rail profile history under different

corrugation initiators will first be developed. A transfer function between initial and final rail profiles in Laplace space will be described and subsequently used to derive a frequency response expression for the corrugation growth mechanism. Results from probability theory are then used to evaluate the expected frequency response due to an arbitrary distribution of pass speeds and from this expression the corrugation growth rate shall be calculated. It is then shown that the growth rate will be maximised under the condition of same speed passes by applying a matrix norm inequality to the frequency response. These theoretical results are then compared against the results of a numerical simulation. Finally an investigation on how the properties of the speed distribution affect the corrugation growth rate and corrugation wavelength will be presented.

2. Corrugation model

2.1. Time-domain model

The variable speed model used in this paper is an extension of the model used in Song and Meehan [14]. The system diagram for this feedback model can be seen in Fig. 1.

This model can generally be described in four stages. The first stage (I) is where the initial rail profile excites the dynamic components of the wheel–rail system. This leads to a variation in contact forces, which in turn affects the contact mechanics (II). The variable contact mechanics leads to a variation in the wear process (III) and this worn rail profile is fed back into this system over successive passages (IV).

This general representation of corrugation formation was used in Meehan et al. [13] to derive a mathematical model by considering a modal description of the dynamics (I), a linear contact mechanics model (II), the frictional work hypothesis to derive a wear relationship (III) and a finite passage delay for the feedback process (IV). A modal description of the wheel/rail dynamics was chosen because experimental and theoretical evidence has shown that the approximately constant corrugation pitch can be associated with a dominant mode of system vibration. This model considers only a vertical vibration mode, but could be extended to account for other modes. The contact mechanics model is based on quasistatic microslip and considers small linear variations about nominal nonlinear operating conditions (see Ref. [15]). The dominant contributions for corrugation growth are assumed to come from the longitudinal components of traction, slip and wear. The wear model is based on assuming that the rate of wear is proportional to the frictional power dissipated.

In Song and Meehan [14] this model was altered by considering an infinite time delay between passages (i.e. the finite pass delay in part IV of Fig. 1 is neglected) to develop an analytic solution of the profile history

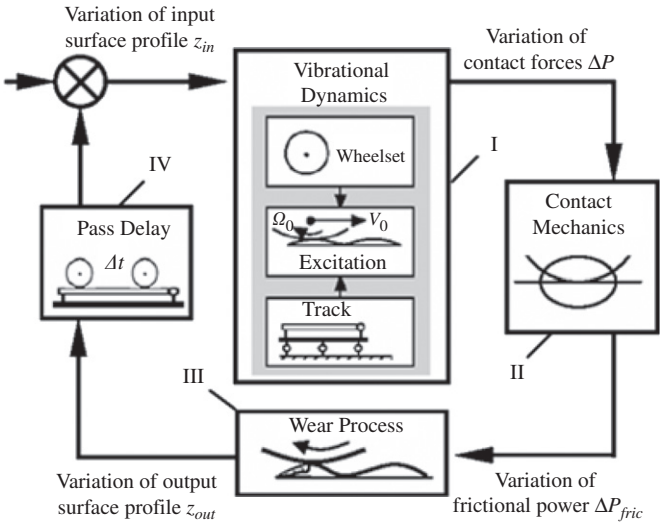

Fig. 1. Feedback model for wear-type rail corrugation.

for multiple wheelsets traversing a bump at the same speed. The present analysis follows a more general derivation, in that the speed may be different on successive passages. This allows insights to be gained into the effect of varying pass speeds for a wide range of initial track profiles. Note that wheel pass frequency effects, as investigated in Meehan and Daniel [16], are not included here in order to clarify the analysis of speed variation effects, but may be investigated at a later date.

A modal description of the coupled wheel–rail dynamics is used to simplify the analysis and can be based on theoretical or experimental models of the real system. Note that this general form allows any mode of vibration (or wavelength) associated with corrugation formation to be modelled. Corrugation growth predictions based on a modal approximation of the dominant wheel/rail mode have previously been validated against both a comprehensive finite element model [13] and field data [17]. As an example of using the dominant mode to model corrugation formation, a two degree of freedom description of the combined wheel–rail dynamics and its modal approximation is provided in Meehan et al. [18]. An outline of this model is given in Appendix A, where a modal decoupling of the vertical dynamics due to the pinned–pinned rail mode and a contact spring is performed to yield a two degree of freedom model of the system, which can be used to highlight the advantages of using a wide distribution of pass speeds. The equations that govern the modal wheel and rail dynamics (representing part I in Fig. 1) are given by

$$\ddot{y}_i + 2\xi_i\omega_i\dot{y}_i + \omega_i^2 y_i = \frac{k_c}{m_i}(p_i - 1)z_{\text{out}_n}(a_n t) \tag{1}$$

for $i = 1$ to M, where M is the number of modes and each y_i is a component of the modal displacement of the wheel/rail system. These relate to the actual wheel and rail displacement by

$$y_w = \sum_{i=1}^{M} p_i y_i \tag{2}$$

and

$$y_r = \sum_{i=1}^{M} y_i. \tag{3}$$

In these equations t represents time, ξ_i is the modal damping ratio, ω_i is the natural frequency, m_i is the modal mass, k_c is the contact stiffness, p_i is the modal contribution factor, z_{out} is the nth pass rail profile and a_n is the ratio of the nth pass speed to the average pass speed.

The equation that describes the wear and contact mechanics (parts II and III in Fig. 1) is given by

$$z_{\text{out}_{n+1}}(t) = K_b\left(\sum_{i=1}^{M}\left[y_{i_{n+1}}\left(\frac{1}{a_n}t\right)(1 - p_i)\right]\right) + \alpha z_{\text{out}_n}(t), \tag{4}$$

where

$$\alpha = 1 + K_b \tag{5}$$

and

$$K_b = \frac{C_\xi k_c \Delta z_0}{P_0}, \tag{6}$$

where P_0 is the steady-state contact pressure, ΔZ_0 is the steady-state wear per pass and C_ξ is the non-dimensional sensitivity of creep variations to contact force variations. An analytic expression for C_ξ is derived from Vermeulan and Johnson creep theory in Ref. [13]. ΔZ_0 can be derived by considering the frictional work hypothesis and in Ref. [13] is shown to be given by

$$\Delta z_0 = \frac{-k_0 \dot{W}_{\text{frict}}}{2b\rho V}, \tag{7}$$

where k_0 is the wear coefficient, ρ is the density, $\dot{W}_{\text{frict}}$ is the steady frictional power, b is the half-width of the contact patch and V is the velocity.

2.2. Transfer function

If the Laplace transforms of Eqs. (1) and (4) are taken, then, after some manipulation, the relationship between the $(n+1)$th rail profile and nth profile in Laplace Space can be shown to be given by

$$Z_{n+1} = A_n Z_n, \tag{8}$$

where

$$A_n = \alpha + \sum_{i=1}^{M} \left(\frac{-K_b K_{c_i}}{a_n^2 s^2 + 2\xi_i \omega_i a_n s + \omega_i^2} \right) \tag{9}$$

and

$$K_{c_i} = \frac{k_c}{m_i}(1 - p_i)^2. \tag{10}$$

Here s represents the usual Laplace Space complex variable, and $Z(s)$ is the Laplace Transform of the rail profile $z(t)$.

A transfer function between the initial rail profile and the nth rail profile in Laplace Space can be derived by solving Eq. (8) for an initial profile Z_0 to give,

$$\frac{Z_n}{Z_0} = \prod_{k=1}^{n} \left(\alpha + \sum_{i=1}^{M} \left(\frac{-K_b K_{c_i}}{a_k^2 s^2 + 2\xi_i \omega_i a_k s + \omega_i^2} \right) \right). \tag{11}$$

Note that Eqs. (1)–(11) are similar to those developed in Song and Meehan [14], except that the variable pass speeds result in a product over the number of passes in Eq. (11), the speed scaling factor a_k has been introduced and the sum over modes has been retained.

2.3. Frequency response

The peak of the frequency response's amplitude ratio as a function of pass number (n) shall be investigated to quantify the growth rate. This is equivalent to the "H_∞ norm" encountered in modern control theory. This measure of corrugation growth is useful because it is relatively simple to derive the frequency response using the transfer function (11) and also because the H_∞ norm has useful properties relating to the magnitude of the corrugated profile when compared against the input profile. For example, it will be equal to the ratio of the induced (worst-case) 2-norms of the output and input profiles in the time domain [19], making it a useful, general measure of the expected corrugation amplitude.

This frequency response peak can also be interpreted in a more simple way as being related to the height of the highest peak of the Fourier Transform of the corrugated output profile (however, caution should be taken with this assumption, as the transients generated from different initial profiles can have a large effect for a small number of passes, as is described in Song and Meehan [14]. These effects become less evident as the number of passes becomes large).

The amplitude ratio of the frequency response of transfer function (11) can be shown to be given by

$$\left| \frac{Z_n}{Z_0}(\mathrm{i}\omega) \right| = \prod_{k=1}^{n} \sqrt{ \left(\alpha + \sum_{i=1}^{M} \frac{-K_b K_{c_i}(\omega_i^2 - \omega^2 a_k^2)}{(\omega_i^2 - \omega^2 a_k^2)^2 + 4\xi_i^2 \omega_i^2 \omega^2 a_k^2} \right)^2 + \left(\sum_{i=1}^{M} \frac{-K_b K_{c_i}(2\xi_i \omega_i \omega a_k^2)}{(\omega_i^2 - \omega^2 a_k^2)^2 + 4\xi_i^2 \omega_i^2 \omega^2 a_k^2} \right)^2 }. \tag{12}$$

If the assumption is made that the modes in the transfer function (11) are independent, then the following simplified expression can be derived:

$$\left| \frac{Z_n}{Z_0}(\mathrm{i}\omega) \right| = \alpha^n \sqrt{ \prod_{k=1}^{n} \left(\frac{(\omega_i^2 - a_k^2 \omega^2 - K_b K_{c_i}/\alpha)^2 + (2\xi_i \omega_i a_k \omega)^2}{(\omega_i^2 - a_k^2 \omega^2)^2 + (2\xi_i \omega_i a_k \omega)^2} \right) }. \tag{13}$$

2.4. Probabilistic speed distribution

It is of interest to examine the behaviour of this frequency response as the number of passes becomes large and when the speeds are distributed randomly. If the ratio of speeds, x, are distributed according to some probability distribution, $p(x)$, then the expected value of the frequency response can be evaluated. The expected value of a general function, $f(x)$, of a random variable, x, with a probability distribution, $p(x)$, is defined by (see for example, Ref. [20])

$$E(f(x)) = \int_{-\infty}^{\infty} f(x)p(x)\,\mathrm{d}x. \tag{14}$$

The expected frequency response can now be derived by considering the ratio of successive passes, which, after some manipulation of Eq. (12), can be shown to be given by

$$\left|\frac{Z_n}{Z_0}(\mathrm{i}\omega)\right| = \exp\left[n\int_{-\infty}^{\infty} \ln\left(\sqrt{\left(\alpha + \sum_{i=1}^{M} \frac{-K_b K_{c_i}(\omega_i^2 - \omega^2 x^2)}{(\omega_i^2 - \omega^2 x^2)^2 + 4\xi_i^2\omega_i^2\omega^2 x^2}\right)^2 + \left(\sum_{i=1}^{M} \frac{-K_b K_{c_i}(2\xi_i\omega_i\omega x)}{(\omega_i^2 - \omega^2 x^2)^2 + 4\xi_i^2\omega_i^2\omega^2 x^2}\right)^2}\right) p(x)\,\mathrm{d}x\right]. \tag{15}$$

If one mode dominates the response then this can be simplified to,

$$\left|\frac{Z_n}{Z_0}(\mathrm{i}\omega)\right| = \alpha^n \sqrt{\exp\left[\int_{-\infty}^{\infty} \ln\left(\frac{\left(\omega_i^2 - x^2\omega^2 - K_b K_{c_i}/\alpha\right)^2 + (2\xi_i\omega_i x\omega)^2}{(\omega_i^2 - x^2\omega^2)^2 + (2\xi_i\omega_i x\omega)^2}\right)\right] p(x)\,\mathrm{d}x}^{n}. \tag{16}$$

The expected frequency response for a large number of passes can now be evaluated by performing the integral in Eq. (15), or in Eq. (16) if the modes are sufficiently independent.

3. Analytic solutions

The transfer function (11) allows the analytic solution to be formed for different initial profiles and for any chosen sequence of pass speeds. In this paper three different profiles are chosen that represent idealisations of what is found in practice; these profiles are a sinusoid, a step and an impulse.

3.1. Solution to sine initial profile

A sinusoidal rail profile can be thought of as an approximation to a train traversing a previously corrugated rail. In the time domain a sinusoidal profile with arbitrary amplitude, A, and angular frequency, b, is given by

$$z_{\mathrm{out}_0}(t) = A\,\sin(bt). \tag{17}$$

In Laplace Space it can be shown that this becomes

$$Z_0 = \frac{Ab}{s^2 + b^2}. \tag{18}$$

Now by multiplying transfer function (11) by initial profile (18), the solution to the nth pass profile can be found by performing a Heaviside expansion (assuming no two passes have exactly the same speed) and then performing an Inverse Laplace Transform. The solution can then be shown to be given by

$$z_{\mathrm{out}_n}(t) = Ab\left\{\begin{array}{l} A_1\,\mathrm{e}^{-\left(\sqrt{-b^2}\right)t} + A_2\,\mathrm{e}^{\left(\sqrt{-b^2}\right)t} \\ + \sum_{i=1}^{M}\left[\begin{array}{l} \sum_{k=1}^{n} \frac{B_{k_i}}{a_k}\mathrm{e}^{-\omega_i\left(\xi_i - \sqrt{\xi_i^2-1}\right)t/a_k} \\ + \sum_{k=1}^{n} \frac{C_{k_i}}{a_k}\mathrm{e}^{-\omega_i\left(\xi_i + \sqrt{\xi_i^2-1}\right)t/a_k} \end{array}\right] \end{array}\right\}, \tag{19}$$

where

$$A_1 = \lim_{s_c \to -\sqrt{-b^2}} w(s_c)\left(s_c + \sqrt{-b^2}\right), \tag{20}$$

$$A_2 = \lim_{s_c \to \sqrt{-b^2}} w(s_c)\left(s_c - \sqrt{-b^2}\right), \tag{21}$$

$$B_{k_i} = \lim_{s_c \to -\xi_i\omega_i/a_k - \omega_i\sqrt{\left(\xi_i^2-1\right)}/a_k} w(s_c)\left(a_k s_c + \xi_i\omega_i + \sqrt{\xi_i^2 - 1}\right), \tag{22}$$

$$C_{k_i} = \lim_{s_c \to -\xi_i\omega_i/a_k + \omega_i\sqrt{\left(\xi_i^2-1\right)}/a_k} w(s_c)\left(a_k s_c + \xi_i\omega_i - \sqrt{\xi_i^2 - 1}\right), \tag{23}$$

and

$$w(s_c) = \frac{1}{s_c^2 + b^2}\prod_{k=1}^{n}\left(\alpha + \sum_{i=1}^{M}\left(\frac{-K_b K_{c_i}}{a_k^2 s_c^2 + 2\xi_i\omega_i a_k s_c + \omega_i^2}\right)\right). \tag{24}$$

Eq. (19) defines the time-domain solution (which can be converted to the space domain solution through the mean velocity) for the whole rail profile for the nth pass. Note that the equations for the coefficients (20)–(23) may appear to go to zero, but the term in brackets will cancel with a term in the denominator of Eq. (24).

3.2. Solution to step initial profile

A step initial profile can be thought of as an idealisation of a wheelset traversing a finite step of a long duration, such as going from one rail section and then onto another that is at a slightly different height (perhaps due to a different rail material hardness). It can also be thought of as an initial displacement perturbation to the wheelset on a flat section of track.

Mathematically this step profile in Laplace Space will be given by

$$Z_0 = \frac{A}{s}, \tag{25}$$

where the step occurs at the time origin and A is the step height. Again by multiplying Eq. (11) by Eq. (25) the nth pass profile in Laplace Space can be found, and by performing a Heaviside expansion and taking the Inverse Laplace transform, the time-domain solution can also be found, giving,

$$z_{\mathrm{out}_n}(t) = A\left\{\frac{A_1}{s} + \sum_{i=1}^{M}\left[\begin{array}{l}\displaystyle\sum_{k=1}^{n}\frac{B_{k_i}}{a_k}\mathrm{e}^{-\omega_i\left(\xi_i - \sqrt{\xi_i^2-1}\right)t/a_k} \\ \displaystyle+\sum_{k=1}^{n}\frac{C_{k_i}}{a_k}\mathrm{e}^{-\omega_i\left(\xi_i + \sqrt{\xi_i^2-1}\right)t/a_k}\end{array}\right]\right\}, \tag{26}$$

where in this case

$$A_1 = \lim_{s_c \to 0} w(s_c)s_c, \tag{27}$$

$$B_{k_i} = \lim_{s_c \to -\xi_i\omega_i/a_k - \omega_i\sqrt{\left(\xi_i^2-1\right)}/a_k} w(s_c)\left(a_k s_c + \xi_i\omega_i + \sqrt{\xi_i^2 - 1}\right), \tag{28}$$

$$C_{k_i} = \lim_{s_c \to -\xi_i\omega_i/a_k + \omega_i\sqrt{\left(\xi_i^2-1\right)}/a_k} w(s_c)\left(a_k s_c + \xi_i\omega_i - \sqrt{\xi_i^2 - 1}\right) \tag{29}$$

and

$$w(s_c) = \frac{1}{s_c}\prod_{k=1}^{n}\left(\alpha + \sum_{i=1}^{M}\left(\frac{-K_b K_{c_i}}{a_k^2 s_c^2 + 2\xi_i \omega_i a_k s_c + \omega_i^2}\right)\right). \tag{30}$$

3.3. Solution to impulse initial profile

The last profile to be considered is an impulse profile. This is an idealisation of a wheelset traversing a small bump or dip of finite duration, such as going over a small weld. Mathematically this will be represented as a delta function, which for convenience will be set at the time origin.

It can be shown that the impulse profile solution will be equal to the time derivative of the time-domain step solution, the only difference being that in this case the coefficient A in Eq. (26) will be given by

$$A = \int_{-\infty}^{\infty} \delta(t)\,\mathrm{d}t. \tag{31}$$

Thus the solution will be given by

$$z_{\mathrm{out}_n}(t) = A\left\{\begin{array}{l} A_1\delta_0(t) \\ -\sum_{i=1}^{M}\left[\begin{array}{l} \sum_{k=1}^{n}\frac{\omega_i\left(\xi_i-\sqrt{\xi_i^2-1}\right)B_{k_i}}{a_k^2}\,\mathrm{e}^{-\omega_i\left(\xi_i-\sqrt{\xi_i^2-1}\right)t/a_k} \\ +\sum_{k=1}^{n}\frac{\omega_i\left(\xi_i+\sqrt{\xi_i^2-1}\right)C_{k_i}}{a_k^2}\,\mathrm{e}^{-\omega_i\left(\xi_i+\sqrt{\xi_i^2-1}\right)t/a_k} \end{array}\right] \end{array}\right\}, \tag{32}$$

where the coefficients are the same as those given in Eqs. (27)–(30).

3.4. Demonstration that same speed passes give an upper bound on corrugation growth

In this section, it is shown that maximum corrugation growth occurs under the case of same speed passes. This is demonstrated by showing that the peak of the magnitude of the frequency response is the highest when same speed passes are used. This useful measure of corrugation growth, as discussed in Section 2.3, can be mathematically interpreted as the maximum of the ratio of 2-norms of the output and input. It follows that different speeds will result in a corrugation growth that is less than or equal to the same speed growth rate.

First, consider that the transfer function for same speed passes between input (initial profile, Z_0) and output (wear after n passes, Z_n) is given by

$$G(s) = \left(\alpha + \sum_{i=1}^{M}\left(\frac{-K_b K_{c_i}}{s^2 + 2\xi_i \omega_i s + \omega_i^2}\right)\right)^n. \tag{32'}$$

Whereas the transfer function for different pass speeds is given by

$$H(s) = \prod_{k=1}^{n}\left(\alpha + \sum_{i=1}^{M}\left(\frac{-K_b K_{c_i}}{a_k^2 s^2 + 2\xi_i \omega_i a_k s + \omega_i^2}\right)\right). \tag{33}$$

An upper bound on the magnitude of the corrugation that develops will be given by the greatest peak in the frequency domain of these transfer functions, i.e.

$$||F(s)||_\infty = \sup_\omega |F(i\omega)|. \tag{34}$$

Now note the result that (see Ref. [21])

$$|(F(i\omega))^n| = |F(i\omega)|.|F(i\omega)|\ldots|F(i\omega)| = |F(i\omega)|^n.0 \tag{35}$$

Therefore if Eq. (32) is written as

$$G(s) = (G_n(s))^n. \tag{36}$$

It can be immediately seen that

$$||G(s)||_\infty = (||G_n(s)||_\infty)^n. \tag{37}$$

This means that (for same speed passes) the frequency peak after n passes is the nth power of the first pass peak. Also note that if the first peak height is greater than 1 (which it is in the typical railroad case because it is under-damped) then the transfer function is unstable in n (as the peak height goes to infinity with n).

Now to make use of the result (see Ref. [19]) that

$$||A(s)B(s)||_\infty \leqslant ||A(s)||_\infty ||B(s)||_\infty, \tag{38}$$

first Eq. (33) is rewritten as

$$H(s) = \prod_{k=1}^{n} H_k(s). \tag{39}$$

Now note that $H_k(s)$ can be scaled such that

$$H_k(p_k s) = G_n(s), \tag{40}$$

thus it can be seen that

$$||H_k(s)||_\infty = ||G_n(s)||_\infty, \tag{41}$$

because a scaling of s will only affect the placement of the peak and not the height. If result (41) is applied into Eq. (38) iteratively we can see that

$$||H(s)||_\infty \leqslant ||G(s)||_\infty. \tag{42}$$

This shows that for a distribution of speeds the upper bound on the peak height is the peak height for same speed passes, and we would generally expect that the peak height would be lower than this upper bound for large n. This proof is valid for a linear model of corrugation formation where the time between passes is large enough that there is little interaction between wheelsets (i.e. it neglects wheel pass frequency effects).

This proof shows that even though different speeds may excite different modes of vibration, the resulting growth rate will always be less than or equal to the variable speed growth rate, provided the frequency domain dynamics do not change with vehicle speed. This assumption may be invalid in the general sense, for example the pinned–pinned resonant frequency may change as the train speed approaches the transverse wave speed of the rail, as discussed in Sheng et al. [22], however, the range of the distribution of speeds will typically only be a fraction of the mean speed and thus any change in the frequency response is only likely to be small over the distributed speed range. Therefore the assumption should be a valid approximation, particularly so for low mean speeds with small variance.

4. Results

The first part of the results section will detail the correlation between these analytic solutions and the outputs given by a numerical straight track simulation, which is described in Meehan et al. [18], where both models use two modes. The second part will show the growth rate reduction predicted by Eq. (16) for three sample probability distributions.

4.1. Comparisons with numerical simulations

To compare the analytic solutions with numerical simulations, the same sequence of randomly generated pass speeds were used in both the numerical model and the analytic model. The coefficients used were generated from realistic physical data, as shown in Table 1. The Fourier transforms of these profiles were then taken, so that the frequency content of the signals could be compared. Some sample plots can be seen in Figs. 2 and 3. These plots show the results obtained for the rail profile in space and frequency domains by

Table 1
Railway parameters for simulation

Mean speed (m/s)	22.22	Track length (m)	6
Wheel mass (kg)	350	Rail density (kg/m^3)	7700
Wheel radius (m)	0.46	Rail radius (m)	0.3
Wheel load (kN)	66	Coeff. of friction	0.4
Young's modulus (steel) (N/m^2)	2.1×10^{11}	Primary rail damping ratio	0.01
Poisson's ratio	0.3	Contact damping ratio	0.0021
Shear modulus (Pa)	7.7×10^{10}	Sleeper spacing (m)	0.6
Sine amplitude (m)	20×10^{-6}	Sine wavelength (m)	0.025
Bump length (m)	0.001	Bump height (m)	100×10^{-6}
Step height (m)	10×10^{-6}	Wear coeff. (kg/N m)	5×10^{-9}
Wear acceleration factor	1000		

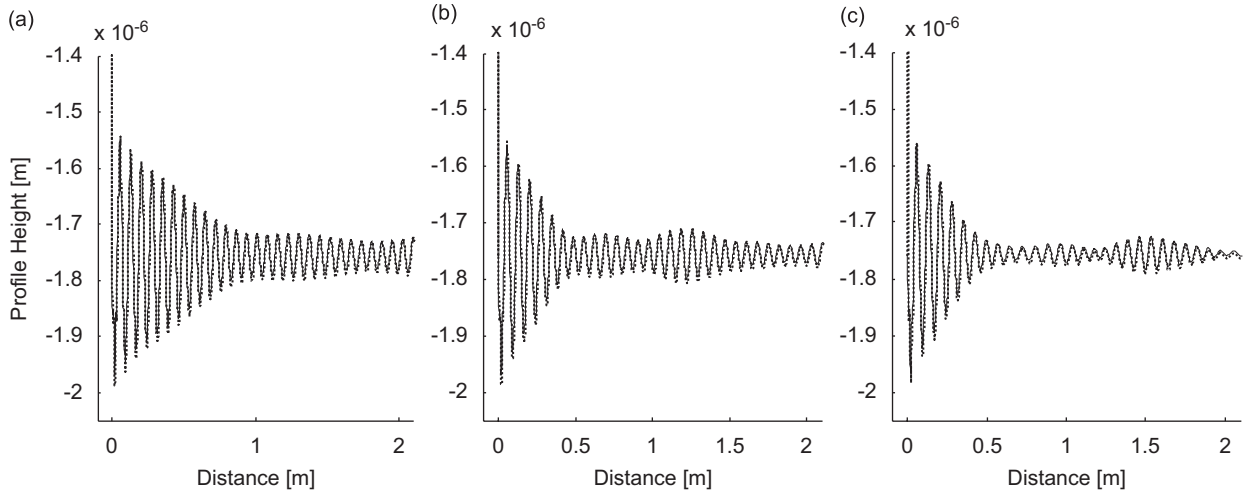

Fig. 2. Numerical (· · ·) and analytic (–) rail profile solutions for impulse profile after 50,000 passes: (a) 2.5%, (b) 5% and (c) 10% standard deviation in speed.

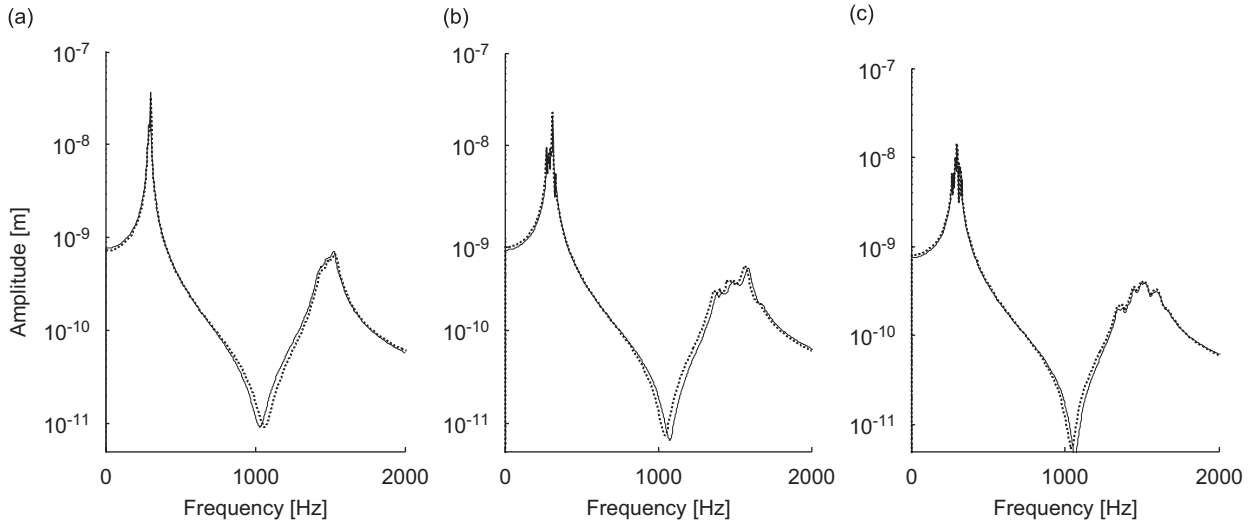

Fig. 3. Numerical (· · ·) and analytical (–) frequency spectra of rail profile after 50,000 passes: (a)–(c) are as in Fig. 2.

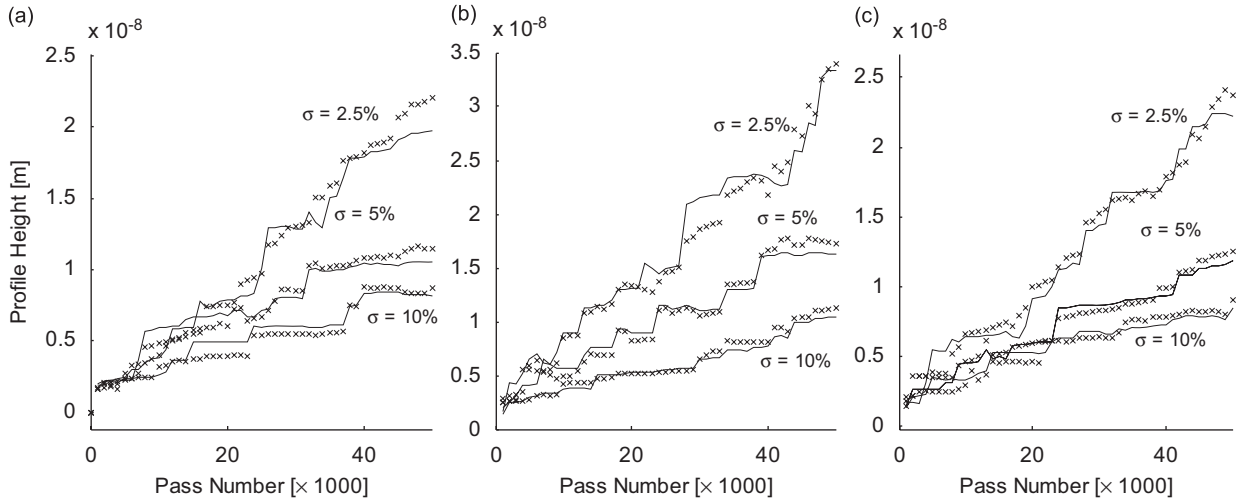

Fig. 4. Peak of frequency spectra for (a) sinusoidal, (b) step and (c) impulse initial profiles for three different speed distributions: (–) analytic and (×) numerical.

using an impulse initial profile. The plots also show speed distributions with different standard deviations in speed, to highlight the effect that speed distribution has on growth rate. Plots of the numerical and analytic solutions are shown overlaid; note that the high degree of correlation makes it difficult to discern the difference between the analytic and numerical solutions.

These plots give a good indication of typical results obtained when comparing these analytical solutions to results from the numerical simulator for the sinusoidal and step profiles, which have been omitted for the sake of brevity. The high correlation between these results gives confidence in the validity of both the numerical methods used and of the approximations used to derive the analytic solution.

To show more detail of the frequency spectra plots and also to highlight the interesting effect that speed distribution has on the growth rate of corrugations, Fig. 4 shows the low frequency peak (at approximately 300 Hz) of the Fourier transform of the output profile for a sequence of normally distributed speeds, but with each having a different standard deviation. This peak was chosen as it is the largest peak due to the dynamic wear. It can be seen that for all the initial profiles considered the same trend is observed that the larger the standard deviation the lower the growth rate. This is investigated further in the next section.

In Fig. 4 there is some difference between the analytic and numerical peak height (particularly for the step profile for a 2.5% standard deviation speed distribution), most likely due to the resolution of the fast Fourier transform. Overall the numerical and analytic results show good agreement for the growth of the highest amplitude peak of the Fourier transform.

4.2. Growth rate reduction

To find out the expected frequency response for a distribution of pass speeds, the integral in Eq. (16) can be evaluated either numerically or analytically. To investigate the growth rate reduction for different distribution properties, three different probability distributions have been examined. They are a uniform distribution, a triangular distribution and a normal distribution.

A uniform distribution gives an equal probability to all pass speeds within a certain range and is defined by

$$p(x) = \frac{1}{c_2 - c_1} \quad \text{for } c_1 \leqslant x \leqslant c_2 \tag{43}$$

and zero everywhere else.

A triangular distribution is defined by

$$p(x) = \begin{cases} \dfrac{2(x-a)}{(b-a)(c-a)} & \text{for } a \leqslant x \leqslant c, \\ \dfrac{2(b-x)}{(b-a)(b-c)} & \text{for } c \leqslant x \leqslant b \end{cases} \tag{44}$$

and zero outside a and b. In Eq. (44) coefficient a represents the lower bound, coefficient b is the upper bound and coefficient c is the mode. In this paper triangular distributions that are symmetrical about the mode have been used.

A normal distribution is given by

$$p(x) = \frac{1}{\sigma\sqrt{2\pi}}\, \mathrm{e}^{-(x-\mu)^2/2\sigma^2}, \tag{45}$$

where σ is the standard deviation and μ is the mean.

To calculate the expected frequency response, Eqs. (43)–(45) can be used in Eq. (16) and the integral evaluated numerically. The peak of the frequency response, which shall be denoted by

$$\left\| \frac{Z_n}{Z_{n-1}} \right\|_\infty = \sqrt[n]{\max_\omega \left| \frac{Z_n}{Z_0}(\mathrm{i}\omega) \right|}, \tag{46}$$

can then be found and plotted against a distribution property. The growth rate G_r is then defined by

$$G_r = \left\| \frac{Z_n}{Z_{n-1}} \right\|_\infty - 1, \tag{47}$$

as in Meehan et al. [13], and as stated previously we can relate this to the worst-case ratio of the 2-norms of the output and input profile, which will grow like,

$$\left(\left\| \frac{Z_n}{Z_{n-1}} \right\|_\infty \right)^n = (1 + G_r)^n. \tag{48}$$

As mentioned previously, for some initial profiles (in particular an impulse profile or a corrugated profile with a frequency close to the expected resonant frequency of the system), this will also describe the growth of the peak of the frequency spectrum of the output profile.

To show the validity of this analysis, Fig. 5 shows the theoretically expected growth rate for a normal distribution versus the distribution's standard deviation (the solid line). Also plotted is the average growth rate obtained from numerical simulations, where an impulse initial profile has been used with the same parameters that are shown in Table 1.

This growth rate was obtained by evaluating multiple runs of 100 accelerated wear passes (equivalent to 100,000 real passes), all generated with normally distributed pass sequences of a fixed standard deviation, and then averaging these growth rates. Similar plots have been obtained for triangular and uniform distributions. It can be seen that there is a good relationship between the theoretical growth rate and the growth rate obtained by the numerical simulations and also that the results are consistent with growth rate predictions in [13] for $\sigma = 0$. Accelerated wear passes have been used (by artificially increasing the wear coefficient) because it significantly reduces computation times and introduces negligible error. Using Eq. (48) it is shown in Appendix B that the error in this assumption can be approximated by

$$\%\ \text{error} \approx 100\left(\frac{n}{2}(F-1)\right) G_r^2, \tag{49}$$

where F is the wear acceleration factor. In these examples the maximum error induced by this assumption will be roughly 0.5%.

To show comparisons between these different distributions a common property of all the distributions is required. The two methods of comparison that have been examined in this paper are matching the variance of the three distributions and matching the width in which 95% of all passes will occur.

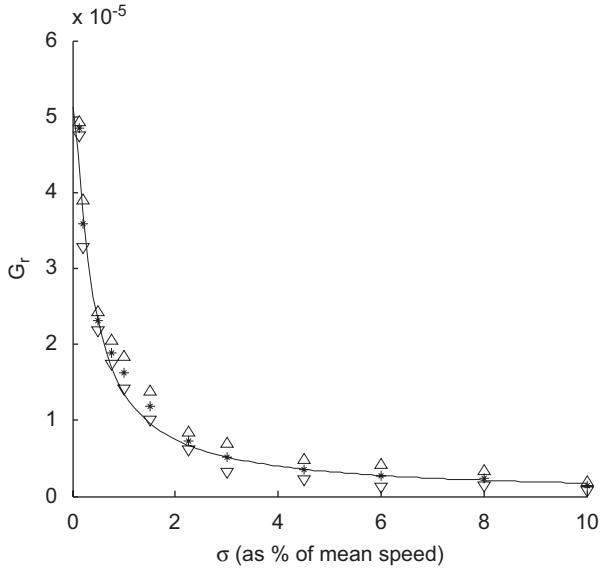

Fig. 5. Growth rate vs. standard deviation: (−) analytical growth rate; (∗) average numerical growth rate; and (△) standard deviation of numerical growth rate.

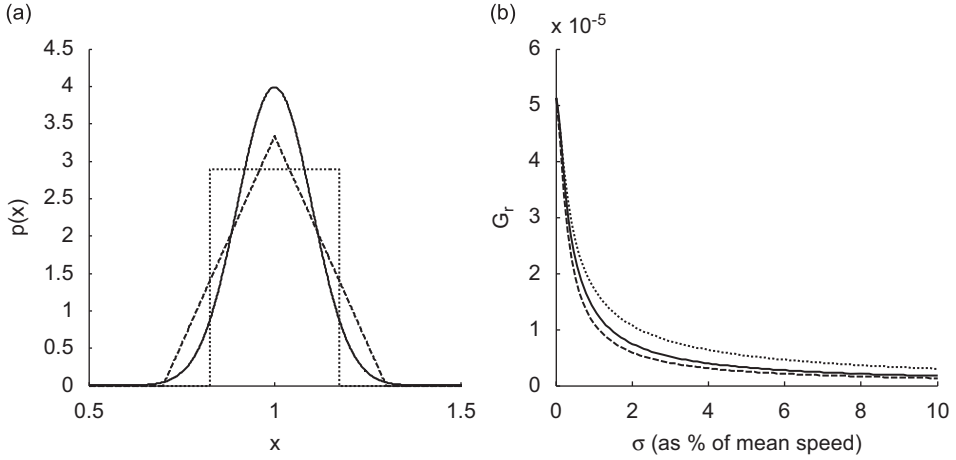

Fig. 6. Probability distributions with matched variance (a) and growth rate vs. equivalent standard deviation (b): (–) normal distribution, (- -) triangular distribution and (· · ·) uniform distribution.

The variance is defined by

$$\sigma^2 = \int (x-\mu)^2 P(x)\,\mathrm{d}x, \tag{50}$$

where σ^2 is the variance and μ is the mean of the distribution. The variance can be thought of as the standard deviation squared.

Fig. 6 shows the distributions when the variances are matched and also shows the expected growth rate reduction for all three of these distributions when considering the variance.

All three distributions share the property that a wider variance results in a lower growth rate, with the greatest reduction being achieved by a triangular distribution and the lowest reduction given by the uniform distribution.

To serve as another basis for comparison of the growth rate reduction, the distributions were compared by matching the width in which 95% of passes will occur. This is intended to give a relative size comparison between the distributions. Fig. 7 shows the three distributions with matched 95% width and the growth rate reduction for the three distributions of equivalent width is shown, which follows the same trend as the matched variance case.

Figs. 6 and 7 show that, for all the distributions considered, the theoretical growth rate can be reduced by a significant amount by increasing the "width" of the speed distributions. As an example of this, consider two sequences of normally distributed pass speeds, with the same mean, but 2% and 4% standard deviations. Using Eq. (48) and the data shown in Fig. 5, it can be shown that it will take approximately two times the number of passes for the corrugation amplitude to reach the same height. The same is approximately true for 4% and 8% standard deviations, etc. Thus a substantial reduction in the theoretical growth rate appears achievable.

It is observed that the broadness of the frequency response peak may reduce the effect of speed variation. This can be seen in Fig. 8 where the growth rate reduction for a normal distribution is plotted for various

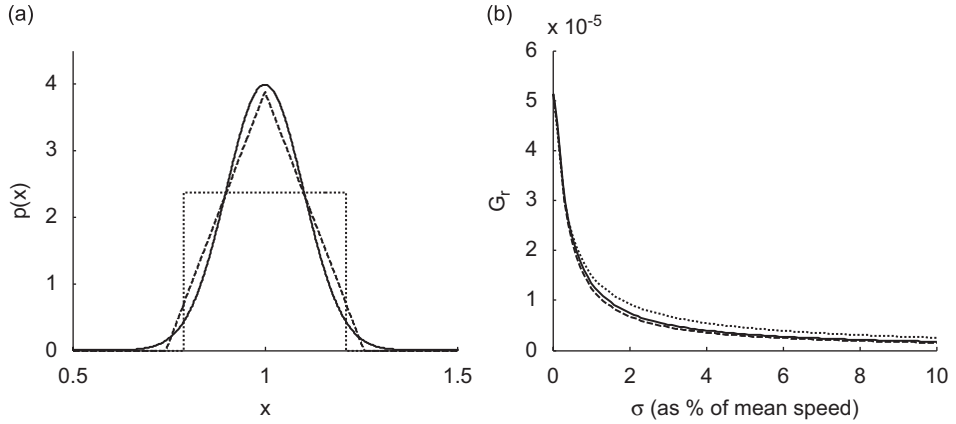

Fig. 7. Probability distributions with matched 95% width (a) and growth rate vs. equivalent standard deviation (b): (–) normal distribution, (- - -) triangular distribution and (· · ·) uniform distribution.

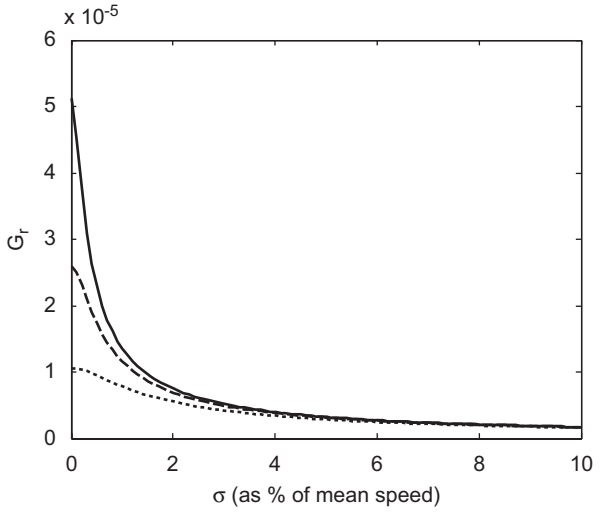

Fig. 8. Growth rate vs. standard deviation for a range of damping values: (–) nominal damping, (- - -) two times nominal damping and (· · ·) five times nominal damping.

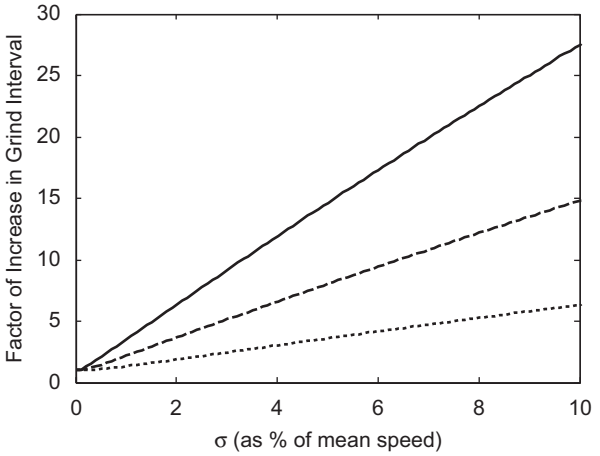

Fig. 9. Factor of increase in grind interval (relative to no speed variation) vs. standard deviation: (–) nominal damping, (- - -) two times nominal damping and (· · ·) five times nominal damping.

damping values. In this figure the damping used in Table 1 has been increased by two and five times, broadening the frequency response.

From this figure it can be seen that speed variation becomes less effective as the damping is increased. This effect can be more clearly seen if the predicted increase in grind interval is considered, that is the factor by which the theoretical time between grind intervals will be increased when compared against no speed variation. For example, if at a certain site there is no speed variation and corrugations reach an amplitude that requires regrinding every year and then speed variation is introduced with a factor of increase f, it will now take f years for corrugations to reach the same amplitude. This factor of increase in grind interval is shown in Fig. 9.

This shows that speed variation will increase the predicted grind interval by a considerable amount, even for the highly damped condition. As an example of the effectiveness of speed variation, the five times nominal damping example will still have a factor of increase in grind interval of approximately three for a 5% standard deviation in speed, which is considerably raised. This would result in grinding costs per annum being reduced to a third of their previous value. It should also be noted that increasing the damping also reduces the growth rate when there is no speed variation, as discussed in Meehan et al. [13].

In reality a specific site will already have a nominal standard deviation in speed, σ, due to driver behaviour and track conditions. The site will also have a corrugation growth rate that is a function of the nominal standard deviation in speed and thus a nominal time for corrugations to reach a certain height. If this standard deviation in speed is increased to $\sigma+\Delta\sigma$, the growth rate will be lowered and the time for the corrugation amplitude to reach a certain height will be increased. The ratio of these two growth times will give a factor of increase in grind interval. This factor of increase in grind interval relative to nominal standard deviation, σ, for a change in standard deviation, $\Delta\sigma$, is plotted in Fig. 10, where contours represent integer values of increase; i.e. twice as long to reach the same height, three times as long, etc.

From this figure it can be seen that it is roughly the case that doubling the standard deviation will double the time for corrugations to reach the same height, which would significantly reduce grinding costs.

It is also of interest to note the influence that speed variation exerts on the wavelength at which corrugations will form. In Fig. 11 the amplitude ratio of the expected frequency response defined by Eq. (16) is calculated for a range of normally distributed speeds.

It can be seen that as the distribution is widened (by increasing the standard deviation), not only does the peak of the amplitude ratio lower but it also shifts the peak's position in wavelength, thus lowering the wavelength of corrugation that would be expected to dominate. This effect is due to each different pass speed effectively making the frequency response of the system more sensitive to a different input wavelength. This means that the system will be less sensitive to the wavelength of corrugation that was previously formed by the last wheelset pass, so that the dynamic feedback mechanism responsible for corrugation growth is disrupted.

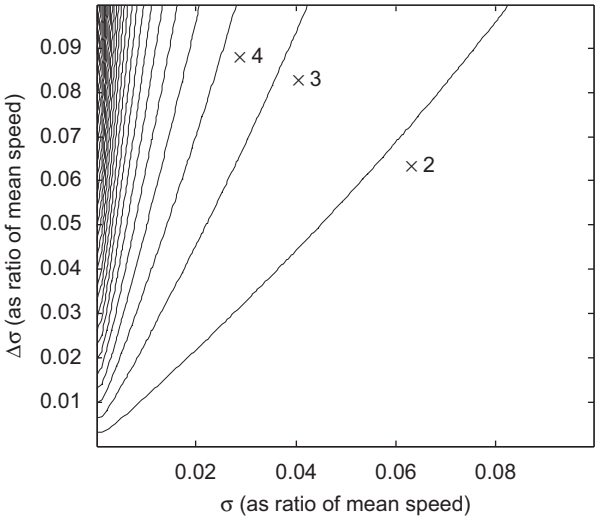

Fig. 10. Nominal standard deviation versus increase in standard deviation for nominal damping case. Contours show integer values for factor of increase in grind interval (e.g. two times as long to reach the same corrugation amplitude, three times as long, etc.).

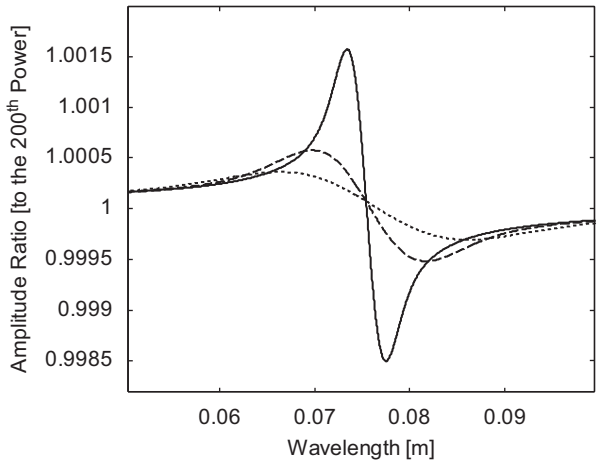

Fig. 11. Amplitude ratio of expected frequency response for a normal distribution: (–) 2% standard deviation, (- - -) 6% standard deviation and (· · ·) 10% standard deviation.

In the long term this leads to a broader wavelength spectrum of corrugation formation with a lower peak height, as each pass creates it own peak at a different wavelength that will be small because the forcing will be more likely to be off resonance.

5. Conclusions

An analytical solution for variable speed passes for three different initial rail profiles has been developed. These solutions show very good agreement with numerical simulations. The frequency spectra of these solutions, obtained by using a fast Fourier transform, are also in agreement. These solutions show that, for all the initial profiles considered, the properties of the probability distribution of speeds has a large effect on the growth rate of the corrugations. A frequency domain expression, derived from the analytic model using probability theory, shows good agreement with the numerical and analytical models and also allows for quantitative analysis of the growth rate reduction. Results of this analysis for realistic parameters indicate that substantial reductions in growth rate may be achieved by increasing the "width" of the speed distribution,

such as by increasing the standard deviation. It has also been shown that increasing the breadth of the frequency response appears to make speed distribution less effective at reducing the growth rate, but large reductions in growth rate still occur. A demonstration has been given showing that same speed passes result in the largest possible corrugation growth rate. Also the effect that speed distribution has on the wavelength at which corrugations may form has been shown.

A possible limitation of the variable speed model as a whole is that it does not take account of nonlinear behaviour, and is thus limited to small amplitude corrugation growth.

While these results show that there is a good correlation between analytical and numerical models, the validity when compared to real systems still needs to be evaluated. This will be tested in studies currently being planned, using both field data and an experimental test rig. Extensions of this work that are under consideration are the investigation of 3D cornering conditions and the inclusion of wheel pass frequency effects.

Acknowledgements

The authors are grateful for the support of the Rail CRC, Queensland Rail, Rail Infrastructure Corporation and the Australian Rail Track Corporation. Thanks are also given to the reviewers for their thoughtful suggestions about the content of this article.

Appendix A

Consider the approximate model for the vertical wheel/rail dynamics given in Fig. 12. Assuming that the wheel is acting like a linearised contact spring and is exciting the first pinned–pinned rail mode, it can be shown via Newton's Laws that the combined dynamics will be given by the following system of equations:

$$m_w\ddot{y}_w + c_c\dot{y}_w + k_c y_w - c_c \sin\left(\frac{\pi e}{L}\right)\dot{q} - \left(k_c \sin\left(\frac{\pi e}{L}\right) + c_c \frac{\pi V}{L}\cos\left(\frac{\pi e}{L}\right)\right) q = k_c h(x) + c_c \dot{h}(x), \tag{51}$$

$$\begin{aligned} &M_1\ddot{q} - c_c \sin\left(\frac{\pi e}{L}\right)\dot{y}_w + \left(C_1 + c_c \sin^2\left(\frac{\pi e}{L}\right)\right)\dot{q} - k_c \sin\left(\frac{\pi e}{L}\right) y_w \\ &\quad + \left(K_1 + k_c \sin^2\left(\frac{\pi e}{L}\right) + c_c \frac{\pi V}{L}\sin\left(\frac{\pi e}{L}\right)\cos\left(\frac{\pi e}{L}\right)\right) q = -(k_c h(x) + c_c \dot{h}(x))\sin\left(\frac{\pi e}{L}\right), \end{aligned} \tag{52}$$

where m_w is the unsprung wheel mass, M_1 is the modal rail mass, c_c is the contact damping, C_1 is the modal rail damping, k_c is the contact stiffness, K_1 is the modal rail stiffness, L is the sleeper spacing, V is the train speed, e is a longitudinal coordinate measured from the first sleeper and $z(x)$ is the rail corrugation profile.

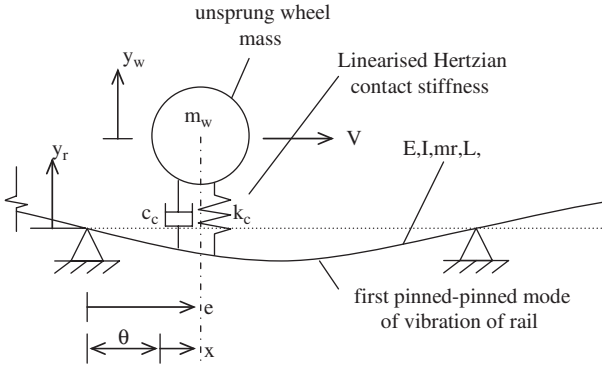

Fig. 12. Schematic diagram representing simplified vertical wheel/rail dynamics.

Now assuming that the system damping is small or approximately proportional and the vibrations are small enough to be regarded as linear, a modal decoupling of the equations of motion can be performed to yield dynamics of the form of Eqs. (1)–(3). Based on the simple two degree of freedom model given by Eqs. (51) and (52) the modal natural frequencies can be found from,

$$\omega_i^2 = \frac{\omega_0^2}{2}\left[1 + \Omega^2(1+M) \pm \sqrt{(1+\Omega^2(1+M))^2 - 4\Omega^2}\right], \tag{53}$$

where the primary natural frequency is that of the pinned–pinned rail natural frequency and is given by

$$\omega_0^2 = \frac{K_1}{M_1} \tag{54}$$

and the non-dimensional mass and frequency ratios are given by

$$\Omega^2 = \frac{M_1 k_c}{m_w K_1} \text{ and } M = \frac{m_w}{M_1}. \tag{55}$$

The modal participation factors used to decouple the equations of motion can be expressed as

$$p_i = \frac{M\Omega^2 + 1 - (\omega_i/\omega_0)^2}{M\Omega^2}. \tag{56}$$

The modal masses may be calculated as

$$m_i = p_i^2 m_w + M_1. \tag{57}$$

Similarly the modal damping can be found from

$$\zeta_i = \zeta_0 \frac{1 + ZM\Omega(p_i - 1)^2}{(\omega_i/\omega_0)(Mp_i^2 + 1)}, \tag{58}$$

where the primary system damping ratio is that of the pinned–pinned rail mode, expressed as

$$\zeta_0 = \frac{C_1}{2\sqrt{M_1 K_1}} \tag{59}$$

and the non-dimensional damping ratio parameter is given by

$$Z = \frac{c_c}{C_1}\sqrt{\frac{M_1 K_1}{m_w k_c}}. \tag{60}$$

Appendix B

To develop the estimate in Eq. (49) for the error in using a wear acceleration factor, consider that the profile ratio over multiple passes is given by Eq. (48),

$$\left(\left\|\frac{Z_n}{Z_{n-1}}\right\|_\infty\right)^n = (1+G_r)^n.$$

To increase the speed of computations the wear coefficient, k_0, is artificially increased by multiplying by a factor F. According to the analytic solution for the growth developed in Ref. [13] the growth rate, G_r, will correspondingly increase, allowing a reduction in the number of passes required, giving

$$\left(\left\|\frac{Z_n}{Z_{n-1}}\right\|_\infty\right)^n_{\text{accel}} = (1+FG_r)^{n/F}. \tag{61}$$

Hence, using Eqs. (48) and (61) the percentage error between the real corrugation growth and the accelerated growth is given by

$$\%\ \text{error} = 100\left(\frac{(1+FG_r)^{n/F}}{(1+G_r)^n} - 1\right). \tag{62}$$

Eq. (62) can be further simplified by looking at a truncated series expansion, which gives Eq. (49).

References

[1] Y. Sato, A. Matsumoto, K. Knothe, Review on rail corrugation studies, *Wear* 253 (2002) 130–139.
[2] K. Hemplemann, K. Knothe, An extended linear model for the prediction of short pitch corrugation, *Wear* 191 (1996) 161–169.
[3] A. Igeland, H. Ilias, Rail head corrugation growth predictions based on non-linear high frequency vehicle/track interaction, *Wear* 213 (1997) 90–97.
[4] A. Matsumoto, Y. Sato, M. Tanimoto, K. Qi, Study on the formation mechanism of rail corrugation on curved track, *Vehicle System Dynamics* 25 (1996) 450–465.
[5] J. Gomez, E.G. Vadillo, J. Santamaria, A comprehensive track model for the improvement of corrugation models, *Journal of Sound and Vibration* 293 (2006) 522–534.
[6] T.X. Wu, D.J. Thompson, An investigation into rail corrugation due to micro-slip under multiple wheel/rail interactions, *Wear* 258 (2005) 1115–1125.
[7] X. Jin, Z. Wen, K. Wang, X. Xiao, Effect of passenger car curving on rail corrugation at a curved track, *Wear* 260 (2006) 619–633.
[8] C. Andersson, A. Johansson, Prediction of rail corrugation generated by three-dimensional wheel–rail interaction, *Wear* 257 (2004) 423–434.
[9] J.J. Kalker, A fast algorithm for the simplified theory of rolling contact, *Vehicle System Dynamics* 11 (1) (1982) 1–13.
[10] A. Bhaskar, K.L. Johnson, G.D. Wood, J. Woodhouse, Wheel–rail dynamics with closely conformal contact, part 1. Dynamic modelling and stability analysis, *Proceedings of the Institution of Mechanical Engineers* 211 (F) (1997) 11–26.
[11] S. Muller, A linear wheel–rail model to investigate stability and corrugation on a straight track, *Wear* 249 (2001) 1117–1127.
[12] J.B. Nielson, Evolution of rail corrugation predicted with a non-linear wear model, *Journal of Sound and Vibration* 227 (1999) 915–933.
[13] P.A. Meehan, W.J.T. Daniel, T. Campey, Prediction of the growth of wear-type rail corrugation, *Wear* 258 (2005) 1001–1013.
[14] N. Song, P.A. Meehan, A closed form analytical solution for a simplified wear-type rail corrugation model, *Proceedings of the ACOUSTICS 2004*, Gold Coast, Australia, 3–5 November, 2004, pp. 227–232.
[15] K.L. Johnson, *Contact Mechanics*, Cambridge University Press, Cambridge, 1987.
[16] P.A. Meehan, W.J.T. Daniel, Effects of wheel passing frequency on wear-type corrugations, *Proceedings of the Seventh International Conference on Contact Mechanics and Wear of Rail/Wheel Systems* (*CM*2006), Brisbane, Australia, September 24–26, 2006, pp. 189–198.
[17] P.A. Meehan, P.A. Bellette, W.J.T. Daniel, R.J. Horwood, A case study on the effect of speed variation on the growth of wear-type rail corrugation, *Proceedings of the 14th International Congress on Sound and Vibration* (*ICSV*14), Cairns, Australia, July 9–12, 2007.
[18] P.A. Meehan, W.J.T. Daniel, T. Campey, Wear-type rail corrugation prediction and prevention, *Proceedings of the Sixth International Conference on Contact Mechanics and Wear in Rail/Wheel Systems* (*CM*2003), Gothenburg, Sweden, June 10–13, 2003, pp. 445–454.
[19] S. Skogestad, I. Postlethwaite, *Multivariable Feedback Control*, Wiley, Chichester, 1996.
[20] J. Galambos, I. Simonelli, *Products of Random Variables*, Marcel Dekker, Inc., New York, 2004.
[21] D.E. Seborg, T.F. Edgar, D.A. Mellichamp, *Process Dynamics and Control*, Wiley, New York, 1989.
[22] X. Sheng, C.J.C. Jones, D.J. Thompson, Responses of infinite periodic structures to moving or stationary harmonic loads, *Journal of Sound and Vibration* 282 (2005) 125–149.